Electron Tomography of Frozen-Hydrated Isolated Triad Junctions

T. Wagenknecht,*[†] C.-E. Hsieh,* B. K. Rath,* S. Fleischer,[‡] and M. Marko*

*Wadsworth Center, New York State Department of Health, Empire State Plaza, Albany, New York 12201-0509 USA; [†]Department of Biomedical Sciences, State University of New York, Empire State Plaza, Albany, New York 12201-0509 USA; and [‡]Department of Biological Sciences, Vanderbilt University, Nashville, Tennessee 37235 USA

ABSTRACT   Cryoelectron microscopy and tomography have been applied for the first time to isolated, frozen-hydrated skeletal muscle triad junctions (triads) and terminal cisternae (TC) vesicles derived from sarcoplasmic reticulum. Isolated triads were selected on the basis of their appearance as two spherical TC vesicles attached to opposite sides of a flattened vesicle derived from a transverse tubule (TT). Foot structures (ryanodine receptors) were resolved within the gap between the TC vesicles and TT vesicles, and some residual ordering of the receptors into arrays was apparent. Organized dense layers, apparently containing the calcium-binding protein calsequestrin, were found in the lumen of TC vesicles underlying the foot structures. The lamellar regions did not directly contact the sarcoplasmic reticulum membrane, thereby creating an $\approx$5-nm-thick zone that potentially constitutes a subcompartment for achieving locally elevated $[Ca^{2+}]$ in the immediate vicinity of the Ca^{2+}-conducting ryanodine receptors. The lumen of the TT vesicles contained globular mass densities of unknown origin, some of which form cross-bridges that may be responsible for the flattened appearance of the transverse tubules when viewed in cross-section. The spatial relationships among the TT membrane, ryanodine receptors, and calsequestrin-containing assemblage are revealed under conditions that do not use dehydration, heavy-metal staining, or chemical fixation, thus exemplifying the potential of cryoelectron microscopy and tomography to reveal structural detail of complex subcellular structures.

INTRODUCTION

In striated muscle, action potentials, initiated at neuromuscular junctions, stimulate contraction by a signal-transduction process known as excitation contraction (EC) coupling. EC coupling occurs at specialized regions where the intracellular sarcoplasmic reticulum forms junctions with the sarcolemma or, more frequently, with tubular invaginations of the sarcolemma known as transverse tubules (Franzini-Armstrong and Jorgensen, 1994; Flucher and Franzini-Armstrong, 1996). In skeletal muscle, a region of transverse tubule (TT) forms junctions with two terminal cisternae regions of the sarcoplasmic reticulum (SR), hence the term triad junction for these regions.

Two multisubunit protein complexes are thought to be preeminent in the mechanism of EC coupling. The dihydropyridine receptor (DHPR), a voltage-activated calcium channel, in the sarcolemmal/TT system functions as the sensor of transmembrane voltage fluctuations, particularly the depolarization wave associated with an action potential. Upon receiving a signal from the DHPR, the ryanodine receptor (RyR) releases Ca^{2+} from the SR into the cytoplasm. Recent studies show that communication between the RyR and DHPR is bidirectional (Nakai et al., 1996, 1998; Grabner et al., 1999). The increased cytoplasmic Ca^{2+} binds to troponin, a component of the muscle filaments that acts as a switch and stimulates muscle contraction. Other protein components occur at triad junctions, and

more continue to be discovered; ostensibly they play either regulatory or structural roles (Mackrill, 1999). For example, calsequestrin, a Ca^{2+}-binding protein that is enriched in the lumen of the SR, probably interacts with RyRs either directly or indirectly via the integral membrane proteins, triadin and junctin. Recently, two additional proteins have been implicated as serving structural roles in the formation or maintenance of TT:SR junctions, mitsugumin (Takeshima et al., 1998; Brandt and Caswell, 1999) and junctophilin (Takeshima et al., 2000).

Current understanding of the three-dimensional ultrastructure of triad junctions from skeletal muscle has come largely from electron microscopy (EM) studies of thinsectioned or freeze-fractured muscle (Franzini-Armstrong and Jorgensen, 1994; Flucher and Franzini-Armstrong, 1996) and of isolated sarcoplasmic reticulum/triad preparations, which preserve interactions among vesicles derived from SR and TTs (Caswell et al., 1976; Mitchell et al., 1983; Kim et al., 1990). From these studies a structural model of the triad junction in vertebrates has been proposed (Block et al., 1988) in which RyRs are arranged on junctional regions of the SR in a two-rowed lattice of variable length, with their large cytoplasmic regions ("feet") located in the gap between the SR and TT membranes. In the TT, DHPRs are arranged in groups of four, called tetrads (Takekura et al., 1994). Each tetrad aligns with an RyR, which itself is a tetrameric assembly. However, only every second RyR is mated with an apposing tetrad. Calsequestrin occupies the lumen of the SR and appears to be attached to the SR membrane by thin cables of uncertain molecular identity.

A more detailed structural model is needed for understanding the mechanism of EC coupling, but progress to-

ward this goal has been slow due to the complexity of the triad junction and the lack of suitable experimental technology. Electron microscopy of triads, either in situ or in isolation, by conventional techniques such as thin sectioning or negative staining fails to resolve reliably structural details in the junctional regions (i.e., between the SR and the TT) other than RyRs. Also, these techniques are prone to well-documented artifacts, associated mainly with dehydration and chemical treatment of the specimen. Recently, it has become feasible to apply electron tomography to frozen-hydrated subcellular structures such as organelles and even whole bacterial cells (Koster et al., 1997; Grimm et al., 1998; Baumeister et al., 1999; Mannella et al., 1999; Nicastro et al., 2000). This approach preserves native structure by rapidly freezing the specimen in a thin aqueous layer by plunging into cryogen, without the use of fixatives or stains (Dubochet et al., 1988). Then, the grid is tilted incrementally over as large a range as possible (typically $\pm 60°$) using a suitably equipped transmission electron microscope, and the images obtained at each angle in the series are combined computationally to produce a three-dimensional reconstruction. Currently, resolutions of 5 to 10 nm are feasible, but significant improvements are predicted (Böhm et al., 2000; McEwen and Marko, 2001). Nevertheless, even with the current technology, novel insights into subcellular organization are possible. Here we describe our initial characterization of isolated triad junctions and terminal cisternae (TC) vesicles by cryoelectron tomography.

MATERIALS AND METHODS

Preparation of specimens for cryomicroscopy

TC vesicles, a fraction of SR-derived vesicles that is enriched in junctional regions of the SR membrane), were isolated as described previously (Saito et al., 1984). Preparations of TC vesicles are also enriched in associated vesicles comprising a TT vesicle and one TC vesicle (dyads) or a TT and two TC vesicles present on opposing faces of the TT (triads). Isolated triads were also prepared by the method of Ikemoto et al. (1988). At the current stage of our analyses, the triads/dyads obtained by the two methods do not display significant differences.

To prepare specimen grids for cryomicroscopy a 3- to 5-μL aliquot of TC vesicles or isolated triads was applied to a 300-mesh grid containing a holey carbon film, blotted with Whatman #40 filter paper, and plunged into liquid ethane (Dubochet et al., 1988; Wagenknecht et al., 1988). Colloidal gold (~15-nm diameter) particles were added as fiduciary markers.

Electron tomography

Tilt series (-60 to $+60°$) were collected at 2°-intervals at an electron dose of 0.5 to 1 electron/$Å^2$ per image (30–80 electron/$Å^2$ total estimated dose per reconstruction). Data were collected using a JEOL JEM4000FX transmission electron microscope operated at 200 kV with objective lens underfocused to 10 μm. At this defocus the first zero of the contrast transfer function is at $(5\ nm)^{-1}$. Both the defocus level and the tilt-angle increment limit the best attainable resolution to 5 to 6 nm. Semiautomated data collection was performed with a TVIPS imaging system implemented as described by Rath et al. (1997). A pixel size of 1 nm was used. Alignment of the projections and three-dimensional reconstruction were carried out using software functions contained within the SPIDER image processing software system (Penczek et al., 1995). No corrections for the contrast transfer function of the microscope were attempted for this study. Six triads were reconstructed for this study. The tomographic volumes were segmented manually using the program STERECON (Marko and Leith, 1996) and rendered as surfaces using IRIS Explorer.

RESULTS

CryoEM of terminal cisternae vesicles and triads

Fig. 1 *A* shows selected micrograph images of frozen-hydrated SR-derived vesicles (see Materials and Methods). Most of the vesicles contain dense material in their lumens, indicating that they are derived from the terminal cisternae regions of the SR, which are those regions that form junctions with TTs (Saito et al., 1984). We refer to these vesicles as TC vesicles. Micrographs of frozen-hydrated TC vesicles show many of the same structural features that were documented previously by negative staining and thin sectioning of resin-embedded, fixed, and stained specimens (Kawamoto et al., 1988). The lumenal density has been attributed to the Ca^{2+}-binding protein, calsequestrin (Jorgensen et al., 1983; Saito et al., 1984). Often the calsequestrin does not fill the entire lumen and is asymmetrically distributed (e.g., left panel, Fig. 1 *A*).

At the exterior edges of the vesicles two types of surface features are visible. Much of the surface has a serrated appearance (Fig. 1 *A*, left and middle panels), which arises from the cytoplasmic regions of the sarcoplasmic Ca^{2+}-ATPase/Ca^{2+} pump, the most abundant transmembrane protein of the SR (Stewart and MacLennan, 1974). Interspersed among the Ca^{2+}-ATPase molecules are rectangular structures (≈ 120 Å normal to the membrane and 300 Å laterally), which often occur in clusters. The rectangular structures are known to correspond to the cytoplasmic regions of RyRs (arrowheads in Fig. 1 *A*) based upon their morphology and immunolabeling (Saito et al., 1988; Kawamoto et al., 1988). These structures are often referred to as junctional "feet" (Franzini-Armstrong, 1980), a term that was coined before their identification as RyRs (Inui et al., 1987). Frequently, the dense lumenal material (calsequestrin) appears to concentrate near regions of the SR junctional face membrane that are enriched in RyRs (e.g., Fig. 1 *A*, left panel).

In a small population of TC vesicles, the dense lumenal material appears paracrystalline (Fig. 1, right panel). The spacing between the rows of dense cables that form these arrays is ≈ 120 Å. Saito et al. (1984) first observed these arrays in TC vesicles that had been prepared for microscopy by noncryo techniques and interpreted them as representing a polymerized polymorphic variant of calsequestrin. Another small population of vesicles has a rather smooth surface and contains little lumenal density material in the interior. These vesicles appear to be derived from the sarcolemma/TT system and are sometimes associated with TC vesicles.

FIGURE 1 Selected examples of frozen-hydrated isolated TC vesicles and triads. (*A*) Selected examples of TC vesicles. In middle panel, a segment of a contaminating collagen fiber is present above the TC vesicle. The dense material in the lumens of the vesicles is attributed to calsequestrin. In some preparations, exemplified by rightmost panel, some of the vesicles contained an apparently organized form of calsequestrin. Arrowheads indicate locations of cytoplasmic regions of ryanodine receptors (feet). (*B*) Three isolated triads. The TC vesicles and TT are indicated in the panels. Ryanodine receptors are sometimes resolved within the junctional gaps (*middle panel*).
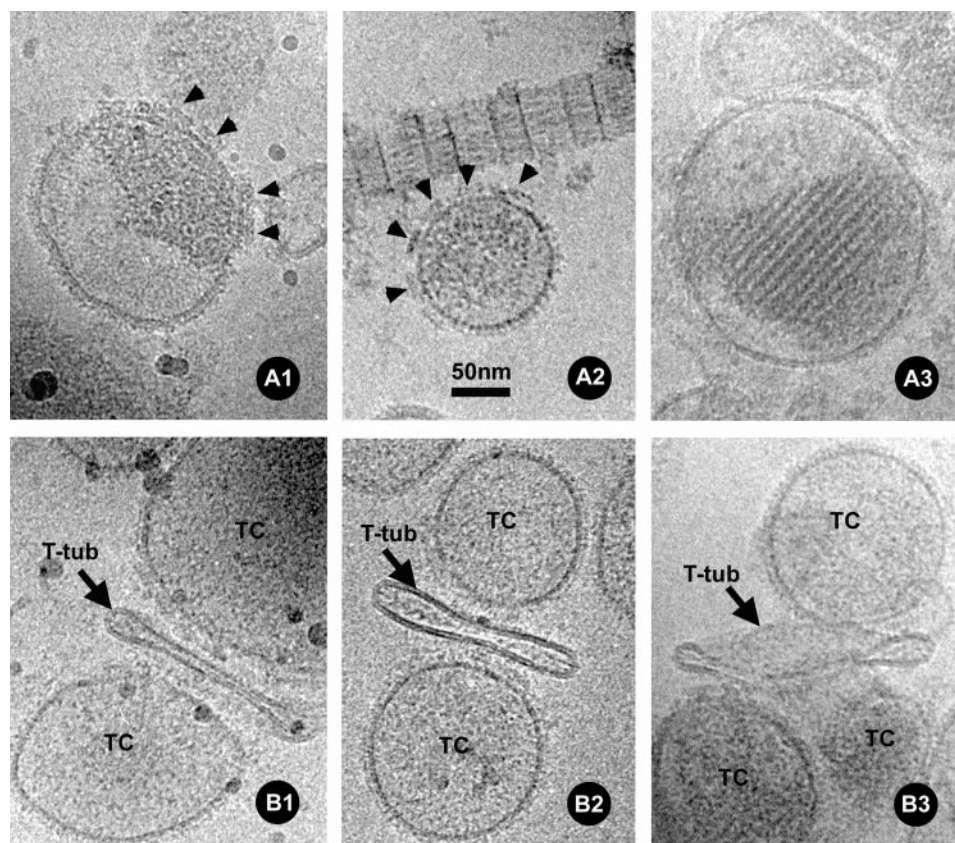
Junctional complexes of TC vesicles and smooth-surfaced vesicles derived from TTs are present at low frequency in preparations of TC vesicles and with higher frequency in microsomal preparations known to be enriched in isolated "triads" (Kim et al., 1983). Sometimes these junctional complexes comprise a flattened smooth vesicle and two SR-derived vesicles attached to it on opposing sides (Fig. 1 *B*), a morphology that is reminiscent of that observed in electron micrographs of triad junctions in transverse sections of skeletal muscle (Franzini-Armstrong and Jorgensen, 1994). Associations of SR- and TT vesicles such as these have been characterized previously by EM of plastic embedded sections and by negative staining (e.g., Brunschwig et al., 1982; Mitchell et al., 1983; Kim et al., 1990). We will refer to them as isolated triads (or dyads in those instances where a TT-vesicle is associated with a single TC vesicle). In thin-section EM such triads and dyads can be overlooked in the micrographs because they occur in orientations in which the TT-vesicle is overlying or underlying an TC vesicle and because vesicles are often crowded together.

Generally, the structural features discussed above pertaining to isolated TC vesicles were also present in the TC vesicles that participated in junctional complexes with TTs. However, because only a small fraction of the TC vesicles were identifiable as participating in junctional complexes, we were not able to select for junctional complexes that occurred in the thinner regions of the ice (<2000 Å) where the contrast is highest. For this reason, and also because the junctional regions may well be more crowded with protein molecules than nonjunctional regions, structural details within the junctional regions tend to be less clear than those of the nonjunctional TC or TT vesicle surfaces.

Despite limited contrast, some structural details are usually discernible in the gap between TT and TC vesicles in junctional complexes. The RyRs/feet are sometimes identifiable due to their high molecular mass (2.3 MDa), although their contrast is usually substantially diminished from that of nonjunctional RyRs (middle panel of Fig. 1 *B*). It should be appreciated that the images represent two-dimensional projections of complex three-dimensional objects, so that tomography is essential for obtaining a more accurate and clearer determination of the mass density distribution in the isolated triads.

Cryoelectron tomography of TC vesicles and triads

Overview

The TC vesicles associated with triads and dyads were heterogeneous in size, but many were less than 150 nm in maximal width. Based upon geometrical considerations and

FIGURE 2 (*A*) Nontilted image of one of the triads that was reconstructed. (*B*) Central *X-Y* section from the three-dimensional reconstruction. The high contrast (*black*) particles are colloidal gold clusters that were added to serve as markers to aid in alignment of the images. Abbreviations as in Fig. 1.
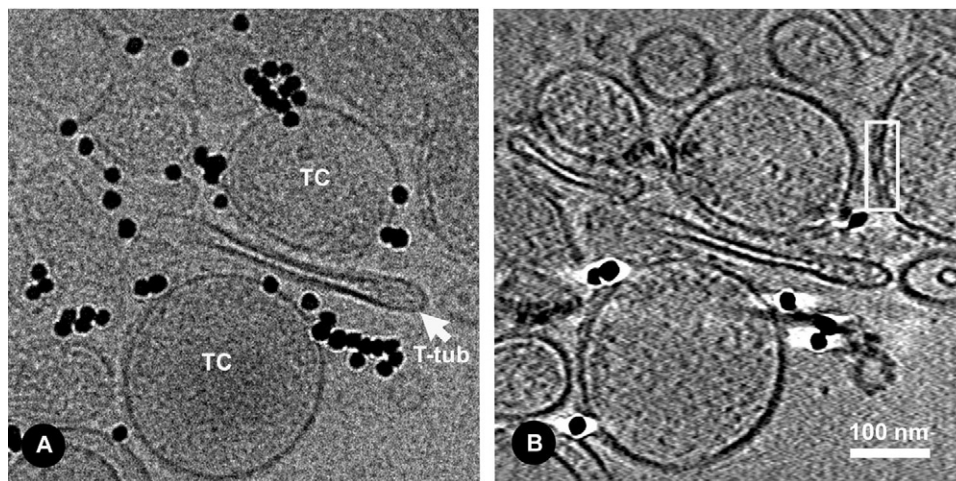
assuming that the vesicles lie in regions of the embedding ice whose thickness approximates the diameter of the largest vesicles, micrographs should be recorded at 2-degree intervals covering 180° to achieve an isotropic resolution of 5 to 7 nm (Crowther et al., 1970). In practice, the tilt range achievable with the specimen holders used in this study is limited to ± 60°, so we collected tilt series at 2° intervals over this range for fields of vesicles that appeared to contain at least one triad. The main effect of the resulting "missing wedge" in the data is that the resolution in the *Z*-direction (defined as the direction along the normal to the plane of the non-tilted specimen) will be reduced. The total electron dose used to collect the series ranged from 30 to 80 electrons/Å^2, a range for which damage from radiation exposure is not expected to be resolution limiting.

Fig. 2 shows one of the isolated triads (triad 3) that was reconstructed for this study. Colloidal gold clusters, 10 to 20 nm in diameter, were added as fiducial markers to aid in the alignment of the micrographs in the tilt series (black particles in Fig. 2). Similar results were obtained for all six of the triads that have been reconstructed. Except where noted otherwise, the discussion that follows is based on the reconstruction of triad 3.

Fig. 3 shows *X-Y* sections spaced at 24-nm intervals through the tomographic reconstruction of triad 3. Note that gold clusters are distributed fairly uniformly throughout the three-dimensional volume. The membranes comprising the TC and TT vesicles are well defined, except at the top and bottom of the reconstruction, where they become increasingly blurred (Fig. 3, panels 1 and 6). The blurring is due largely to the missing wedge of data, an effect that has been described previously for lipid vesicles and mitochondria (Dierksen et al., 1995; Nicastro et al., 2000). Inspection of the sections reveals that the reconstructed volume contains a second, smaller triad (visible in panels 4 and 5 to the left of the larger triad) that was not readily identified in the tilt-series micrographs.

The width of the gap between the TC and TT vesicles in the junctional regions was measured at multiple locations in each of the reconstructed triads. The distance between the centers of the membranes was found to be 19.5 ± 1 nm in the regions where the membranes were most closely associated (which coincided with regions containing junctional feet, as discussed further below). Allowing for the thickness of the bilayers, the actual gap between the TC and TT membranes is estimated at 15.5 ± 1 nm.

Substructure in lumen of SR

As was discussed in the previous section, images of SR vesicles indicate the presence of dense granular material in their lumens apparently corresponding to calsequestrin, the major lumenal protein. The tomographic reconstructions show evidence of additional structural organization of this dense material. Inspection of the individual *XY* slices (Fig. 3) reveals discrete foci of density. Comparison of intralumenal areas with regions outside of the vesicles indicates that these densities are significantly above the background noise. The background density within much of the SR lumen does not differ greatly from that in regions outside of the vesicle; this contrasts with tomographic results on mitochondria that showed the mitochondrial matrix to have an overall density that was higher than exterior regions (Nicastro et al., 2000). Apparently, the mitochondrial matrix is more densely packed with protein than are the TC vesicles.

A three-dimensional representation of the tomogram determined for triad 3 is shown in Fig. 4. This "surface representation" was created by tracing interactively the membrane bilayers and RyRs/feet and by identifying the locations of the SR lumenal densities and representing them as spheres approximating their average diameter. It should be emphasized that this representation of the triad is an oversimplification of the actual density distribution in the reconstruction. For example, the SR lumenal densities
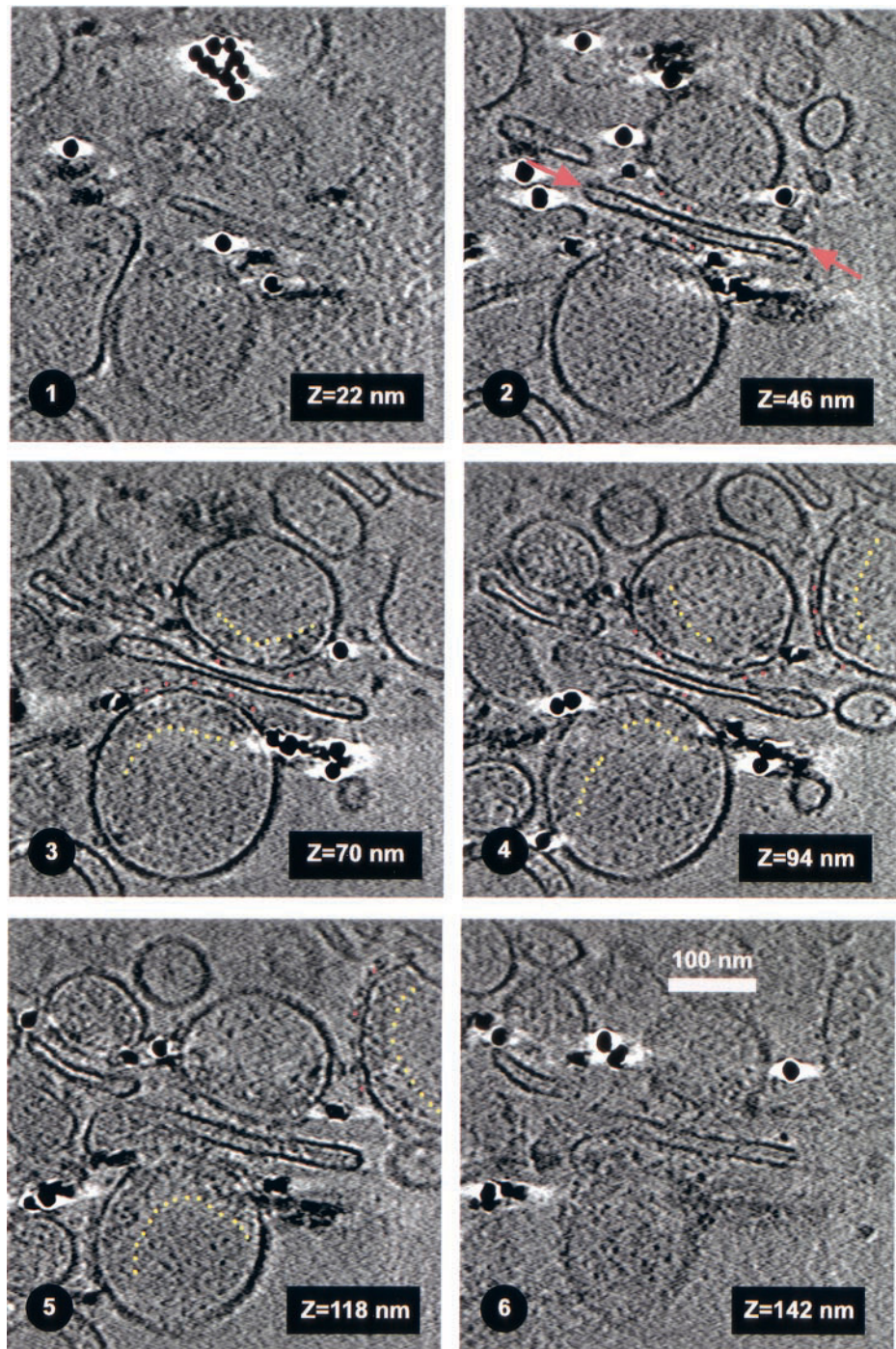
FIGURE 3 Selected *XY*-slices from to-mographic reconstruction of triad 3. The *Z*-coordinate of each slice is indicated in lower right corner. Orange dots denote locations of RyRs (feet); yellow dotted lines are drawn to indicate regions of organized calsequestrin located between the dotted line and the SR membrane. The TC vesicle at upper right in panels 4 and 5, which is not part of the triad, contains particularly well-resolved RyRs and underlying organized calsequestrin. Notice that the colloidal gold clusters are present in all slices, indicating that the clusters are distributed uniformly throughout the layer of vitreous buffer in which the triads are embedded.

(calsequestrin) are not always spherical in shape as indicated, and frequently there appears to be additional density that interconnects these densities that is too faint to trace reliably and is therefore not indicated in the surface representation.

Interestingly, the lumenal high-density regions in the TC vesicles appear much more densely packed and organized near the membrane surface, specifically at regions where multiple RyRs are present. Several of these regions are outlined by dotted lines in Fig. 3 (panels 3–5). Sometimes a nearly continuous sheet of density, several tens of nanometers in thickness, underlies the SR membrane. The detailed structural features in these regions are difficult to discern fully, so in the surface-rendered representation of the triad we indicate only the approximate boundaries of these regions (Fig. 4, yellow shading).

These regions of organized lumenal density appear not to contact the surface of the SR membrane. Rather, there is a

FIGURE 4 Surface-rendered representation of triad 3 in stereo. SR- and TT-derived vesicles in green and red, respectively. Yellow spheres in lumen of SR represent calsequestrin and continuous yellow slabs near junctional surfaces of SR represent the condensed calsequestrin (see Fig. 3). Blue structures correspond to feet/RyRs. Magenta particles in lumen of TT are of unknown identity.
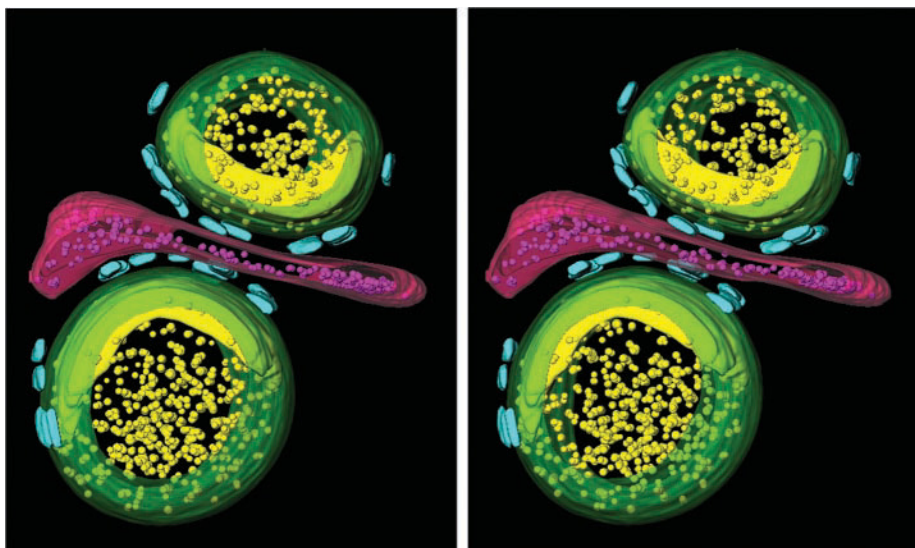
zone of reduced density ≈5 nm in width between the lumenal density and the SR membrane (this is particularly well-resolved in the nonjunctional TC vesicle on the right side of panel 4 in Fig. 3). This "clear" zone is apparently not an electron-optical artifact, because it is much less prominent on the exterior surface of the SR membrane. Furthermore, cryotomograms of mitochondria, determined by similar procedures to those we have used, do not show such low density regions associated with their inner membrane and cristae even though the mitochondrial matrix is densely packed with protein (Mannella et al., 1999; see also Nicastro et al. 2000). Densities that bridge the gap between the region of high density and the SR membrane sporadically interrupt the clear zone.

T-tubule

Although structural details are not reproducibly resolved on the exterior membrane surfaces of the TT vesicles, the lumens of the vesicles contain particulate densities, particularly in the widest portions, outside of the junctional regions. The locations and approximate sizes of the TT lumenal densities are indicated in the surface-rendered model of triad 3 (purple areas in Fig. 4). In some regions the densities appear to form cross-bridges that extend across the width of the TT (e.g., panels 2 and 5 of Fig. 3). Perhaps these structures are involved in establishing the distinctive flattened shape of the TT vesicles.

Exterior surface of TC vesicles: nonjunctional and junctional regions

The *X-Y* sections shown in Fig. 3 show TC vesicles containing high-density regions on their exterior (cytoplasmic-facing) surfaces whose size and shape indicate that they correspond to the cytoplasmic domains of RyRs (i.e., feet,

indicated by orange dots in Fig. 3) that have been observed in previous EM studies of sectioned muscle and isolated SR-derived vesicles (Caswell et al., 1976; Mitchell et al., 1983; Kim et al., 1990; Franzini-Armstrong and Jorgensen, 1994; Flucher and Franzini-Armstrong, 1996). Frequently, the feet appear disconnected from the SR membrane to which they are apparently attached via the RyR's transmembrane region. In junctional regions, visible connections between the feet and TT membrane are also infrequent (however, see below), and consequently the feet often appear to be "floating" between the SR and TT membranes. This appearance of the feet is also conveyed in the surface rendered representation of the triad (blue regions in Fig. 4). The feet that occur outside of junctional regions probably arose during the homogenization step of the isolation procedure, as most RyRs are thought to be associated with the TT/sarcolemma membrane system in situ.

Individual Ca^{2+}-ATPase molecules are not well resolved from one another in the reconstructed triads, but the nonjunctional regions of the TC appear thicker, denser, and less smooth on their exterior faces, which is consistent with these regions being densely packed with Ca^{2+}-ATPase.

The junctional regions between TC and TT vesicles are of particular interest. However, besides the RyRs, little substructure is reliably resolved in these regions. The cytoplasmic domains of RyRs are readily identifiable in the gap between the vesicles, although they are less well contrasted than in nonjunctional regions of the TC vesicles, probably due to the presence of other proteins in the junctional gap. The locations of the RyRs that were identified on the two TC vesicles in triad 3 are indicated in Fig. 4 (blue structures). Most of the RyRs in this reconstruction are localized at or near regions of the TC vesicles that interact with TT vesicle, but not all appear close enough to the surface of the

TT vesicle to directly interact with it. Most of the RyRs in each of the two junctional regions are constrained to a narrow band that may represent the remnant of a two-rowed array of the type observed in electron micrographs of freeze-fractured or thin sectioned images of intact muscle (Ferguson et al., 1984).

A clearer example of RyRs forming a two-rowed array is found in one of the nonjunctional TC vesicles that were present adjoining triad 3 (upper right in Fig. 3, panels 4 and 5). A subvolume extracted from this region, when viewed in projection, shows apparently three well-resolved RyRs (Fig. 5). When this region of the three-dimensional volume is viewed at a 90° angle, onto the exterior surface of the TC vesicle, it becomes apparent that six RyRs are actually present and that they are arranged in a two-rowed array of the type observed previously by EM of intact muscle (Fig. 5B). The handedness of the array is also revealed by the reconstruction, and it agrees with the handedness that we observed previously for oligomers comprising two or three RyRs that sometimes occur in preparations of purified RyRs (Wagenknecht et al., 1997).

In junctional regions, there often appears to be a gap of several nanometers between the distal face of the feet and the surface of the TT vesicle (see RyRs in junctional regions in Fig. 3, panels 2–4). Because the nature of the linkage between the RyRs and TT-associated voltage sensor (the DHPR) is thought to be critical for understanding the mechanism of EC coupling, we have examined all of the junctional RyRs in the reconstructions. Some of the RyRs appeared to be associated with density linking them to the TT vesicle (Fig. 6). The number of connections per RyR varies between zero and three, with zero or one being the most common. In some cases the density occurs in regions where the gap between TC and TT vesicle is greater that 16 nm (lower rightmost panel in Fig. 6). The bridging densities may correspond to cytoplasmic regions of the DHPRs, but further studies are required to determine their molecular identity.

DISCUSSION

We have described here the first results of cryo-EM and tomography of triad junctions. Since gaining popularity in the 1980s, EM of frozen-hydrated solutions of isolated macromolecules has become the standard method for characterizing the ultrastructure of large multisubunit biological structures such as ribosomes, viruses, and membrane-associated proteins (e.g., Agrawal and Frank, 1999; Chiu et al., 1999; Baumeister and Steven, 2000; Nogales and Grigorieff, 2001). There is widespread agreement that this technique, which does not require the use of stains, fixatives, or dehydration, is capable of preserving macromolecular structure to atomic resolution. However, one drawback of the technique is the poor contrast exhibited by ice-embedded specimens. For isolated multisubunit protein or nucleic ac-
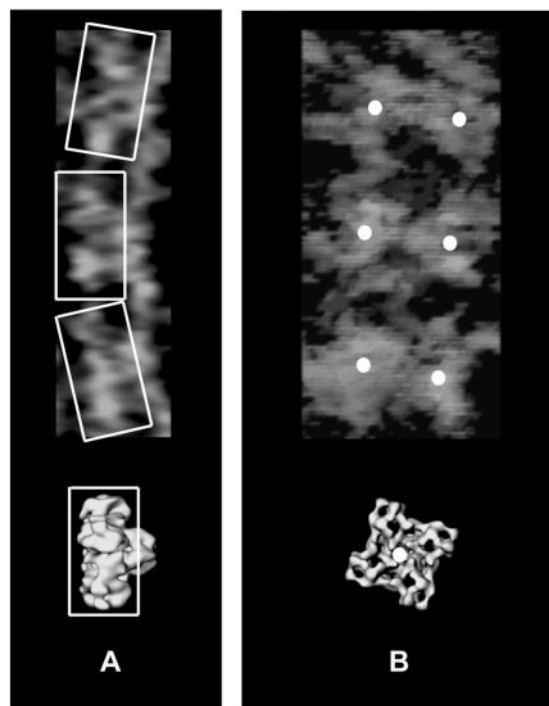
FIGURE 5 Evidence for arrays of ryanodine receptors. (A) Enlarged view of the cluster of ryanodine receptors shown on right side of Fig. 3 (panels 4 and 5) as seen in projection in a subvolume extracted from the tomographic reconstruction. For comparison, at the bottom is shown a reconstructed ryanodine receptor as determined previously by single-particle image processing of purified receptors (Radermacher et al., 1994). Note that contrast is reversed from previous figure: protein density is white. (B) En face view of the cluster of ryanodine receptors. When the subvolume in the orientation shown in A is projected following rotation of 90° about the vertical, it becomes clear that the cluster of receptors comprises two rows of receptors (six in total). A single-particle reconstruction of the receptor in the en face view is at the bottom. Double-rowed arrays of this type have been detected previously by the freeze-fracture technique (Block et al., 1988).

id/protein complexes this problem can be overcome by averaging over images obtained from thousands of particles, but averaging is not feasible for subcellular structures, such as the isolated triads, which are not homogeneous with regard to their overall sizes and shapes. In electron tomography a limited number of images of a single subcellular structure or region is obtained by tilting incrementally the specimen, and these are combined to produce a three-dimensional reconstruction. Although the contrast of the reconstruction is improved over that present in the unprocessed images, it is still not optimal for making detailed interpretation of the density maps.

Here, isolated triads were chosen for tomography rather than triad-containing regions of intact muscle because sectioning frozen tissue is technically difficult and produces compression artifacts (Ruiz et al., 1994; Dubochet and Sartori Blanc, 2001; Hsieh et al., 2002). Further, the contrast of triads in frozen-hydrated sections would doubtless be
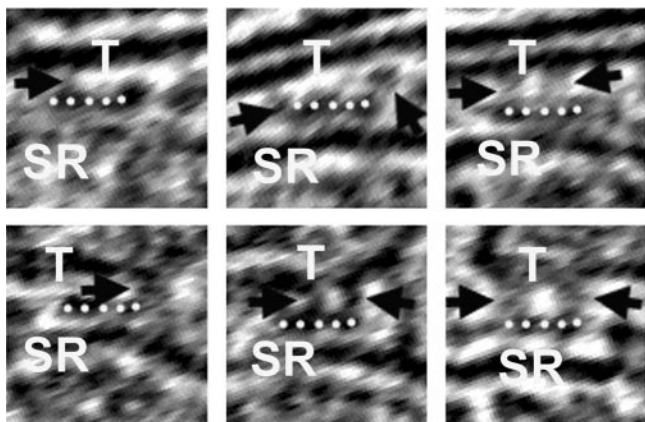
FIGURE 6   Ryanodine receptor t-tubule interactions. Selected examples of RyRs that appear to be linked to the TT. Arrows indicate the locations of density that bridges the gap between the RyR/foot and the TT membrane. Dotted lines mark the cytoplasmic regions (feet) of RyRs. Locations of TT (T) and junctional SR membranes are also indicated. Arrows indicate connections between ryanodine receptors and TTs, which bridge the ≈ 4-nm gap between the RyR and the TT. Regions of high protein or membrane density are dark.

even lower than that found for isolated triads. Moreover, observations showing that isolated triads retain the basic structural features of the triad junction and are functional, in the sense that chemical-induced depolarization of the TTs induces release of Ca^{2+} from the associated SR vesicles, indicate that isolated triads represent a valid model system for elucidating the mechanism of EC coupling (Anderson and Meissner, 1995; Corbett et al., 1992; Ikemoto et al., 1984; Kramer and Corbett, 1996). Isolated triads offer several properties that are favorable for cryoelectron microscopy and tomography: 1) contrast is maximized because they can be imaged in thin (150–300 nm) films of buffer and in the absence of nontriad cytoplasmic proteins; 2) many of the triad's protein components are readily accessible for immuno-labeling; 3) experimental conditions can be varied readily and tested for functional consequences in parallel with structural characterization. As discussed in detail below, our initial reconstructions reveal some new ultrastructural features that point to the promise of cryoelectron tomography.

Comparison with previous results on the ultrastructure of the triad junction

A model for the three-dimensional architecture of the vertebrate skeletal muscle triad junction has been proposed by Franzini-Armstrong and her colleagues (Block et al., 1988). This model is based upon results of numerous morphologic studies using various EM techniques (for reviews, see Franzini-Armstrong and Jorgensen, 1994; Franzini-Armstrong, 1994; Flucher and Franzini-Armstrong, 1996). In this model, RyRs are arranged on the junctional-face membrane

of the SR as an ordered, two-rowed array whose length is variable. An intriguing feature of the model is that the DHPRs in the TT are disposed as groups of four (called tetrads) whose members align with the subunits of the four-fold symmetric RyRs in the apposed SR membrane (Block et al., 1988). However, the pairing of tetrads with RyRs appears to occur in an alternating pattern, such that only one-half of the RyRs are paired with tetrads. This precise alignment of the two receptor types suggests a physical interaction between them, which is consistent with the currently favored "mechanical coupling" mechanism of EC coupling in skeletal muscle whereby a voltage-dependent conformational change in the DHPRs induces opening of those RyRs in direct contact with them. Another feature of the Franzini-Armstrong model is that calsequestrin is concentrated in the cisternae of the junctional SR, but appears not to extend to the inner leaflet of the SR membrane. Thin strands of material, which could contain one or both of the proteins, triadin and junctin (Zhang et al., 1997), anchor the calsequestrin to the SR membrane. Many additional proteins are known (Costello et al., 1986) or hypothesized to be present at the triad junction, but their locations, interaction partners, and stoichiometry are unknown (Mackrill, 1999). Also, there is considerable uncertainty about some of the basic architectural features of the model. For instance, reports of the width of the gap between the SR and TT membranes range from 10 to 20 nm. The studies described here provide a path to refine and extend this model for the triad junction, which is essential for elucidating the mechanisms of EC coupling.

The structural organization of the gap between the TT and SR junctional face membranes in the triad junction (triadic gap) is of particular interest, because events associated with communication between the two membrane systems are likely to occur there. The only structural feature that has been definitively identified in the triadic gap corresponds to the large ($M_r \approx 2 \times 10^6$), fourfold symmetric cytoplasmic region of the RyR, the so-called junctional "feet." Our reconstructions also show these structures.

One difference exhibited by our three-dimensional reconstructions from previous microscopy studies of skeletal muscle or isolated triads prepared by thin sectioning is that the majority of the feet do not appear to physically contact the TT. Instead, a gap, several nm in width, exists between the TT and RyR. Consequently, the total width of the junctional gap is 15 to 16 nm, significantly greater than the 12-nm width of the cytoplasmic region of the RyR (Serysheva et al., 1995; Radermacher et al., 1994). Previous estimates of the width of the triadic gap have ranged from 10 to 20 nm (Franzini-Armstrong, 1994). Some of the feet appear to be connected to the TT via bridging density (Fig. 6). Possibly these bridging densities correspond to domains or subunits of the DHPRs that are believed to directly interact with the RyRs. However, we have not observed a case where four symmetrically arranged bridging structures

interact with a RyR, as would be expected if they corresponded to the tetrads that have been observed in micrographs of TT derived membrane by the freeze-fracture technique (Block et al., 1988).

Although we cannot be certain that the 15- to 16-nm junctional gap that we have observed is not artifactually large as a consequence of structural rearrangements that might occur upon homogenization of muscle tissue and isolation of the triads, several considerations argue against this possibility. As mentioned earlier, isolated triads exhibit EC coupling activity in vitro, and this activity is expected to be sensitive to disruption of the linkage between the TT and SR. Also, biological material prepared for microscopy by conventional thin-sectioning techniques suffers from shrinkage and other potential artifacts, which could account for the more compact appearance of the triad junction in some of these preparations. Finally, recent structural characterizations of voltage-gated potassium and sodium channels (Gulbis et al., 2000; Kobertz et al., 2000; Sokolova et al., 2001; Sato et al., 2001), which are related to the DHPR, indicate that folded domains of the channels contribute significant mass on the cytoplasmic side of the membrane. If similar or analogous cytoplasmic domains exist for the DHPR, then they would suffice to bridge the 3- to 4-nm distance between the distal face of the RyR and the surface of the TT membrane, which is consistent with our observation of density apparently connecting some RyRs to the TT (Fig. 6).

Much of the dense material occupying the lumen of the junctional SR vesicles is attributable to the protein calsequestrin, the most abundant lumenal protein (Saito et al. 1984; Maurer et al., 1985). Our tomographic reconstructions show a dense layer of protein (which we presume to be calsequestrin based on evidence summarized by Franzini-Armstrong and Jorgensen (1994)), just beneath the SR membrane and primarily in regions that contain RyRs. These subsarcolemmal regions are variable in size, but they do not extend more that a few tens of nanometers into the interior of the lumen. Tomography was necessary to reveal this distribution of the density, as it was not apparent in the micrographs themselves. The distribution of globular structures that comprise these regions gives the impression of structural organization (Fig. 3). There are also isolated punctate regions of high density deeper within the lumen of the SR vesicles (small yellow spheres in Fig. 4). These densities may represent monomeric or oligomeric clusters of calsequestrin molecules that co-exist with the larger SR membrane-associated assemblages.

Interestingly, the calsequestrin-enriched regions do not appear to interact directly with the SR membrane, but rather a zone of reduced density of ~5-nm thickness occurs between the SR membrane and the calsequestrin. Sometimes, faintly visible bridges of density between the SR and the organized calsequestrin interrupt the "clear zone." In the model of the triad junction proposed by Franzini-Armstrong

(Block et al., 1988; Franzini-Armstrong and Jorgensen, 1994), the calsequestrin also forms a lumenal aggregate that is linked to the SR membrane by thin strands of protein. The width of the gap has been uncertain, because different EM preparation methods have yielded discordant results (Brunschwig et al., 1982; Franzini-Armstrong et al., 1987). Because cryotomography does not require dehydration or fixation, we are confident that the ~5-nm-thick zone of reduced density between the SR and the organized calsequestrin reflects the native architecture. This zone could be of functional significance for calcium release from the SR, perhaps by maintaining an appropriately high level of Ca^{2+} ions in the immediate vicinity of the RyRs' ion-conducting channels.

The TTs in frozen-hydrated preparations of triads appear as flattened vesicles that are wider at their perimeter. They are most flattened in regions that form junctions with the SR-derived vesicles with the separation between bilayers in the narrowest zones approaching 10 nm. Mass density within the lumen is lower than for SR vesicles and is concentrated in the wider, peripheral regions. These findings generally agree with observations made by noncryo EM of isolated triads (Brunschwig et al., 1982; Kim et al., 1990; Mitchell et al., 1983). Some high-density regions were observed in the more flattened regions of the TT, sometimes giving the appearance of forming cross-bridges linking apposing bilayers. These structures have not been described in previous ultrastructural studies of isolated triads or in studies of sectioned muscle, except for one report by Dulhunty (1989) who observed similar structures in lightly fixed and stained specimens and termed them "tethers." In agreement with previous studies, we find that the cytoplasmic surfaces of the TT bilayer (the exterior side in the isolated triads) appear much smoother than those of the SR vesicles.

Outlook

The isolated triad junctions that we have reconstructed by cryoelectron tomography have likely retained their native architecture to a degree that has not been achieved in previous microscopy studies. However, the inherent low-contrast and radiation sensitivity of nonstained, nonfixed biological specimens limit the information content of reconstructions determined by current implementations of the technique. The resolution attained for the triads described here are not known precisely, but is unlikely to be better than 6 nm in the *X-Y* direction and poorer in the *Z*-direction (normal to the specimen grid). Even so, as discussed above, several features are present in the tomograms that are either novel or support unsubstantiated previous observations.

We are optimistic that future investigations by cryoelectron tomography will provide much more detailed structural information on the triad junction, quite possibly at a level that cannot be obtained by any other approach. Improve-

ments and enhancements to electron microscopes, data-collection strategies, and image-processing methods are expected to permit resolutions of 2 to 4 nm to be attainable (Koster et al., 1997; Böhm et al., 2000). In this resolution realm it should be possible to identify multisubunit protein assemblies whose structures are already known (e.g., from x-ray crystallography or EM of the isolated complexes) on the basis of their density distribution alone. In the case of triads, RyRs are already identifiable, and their coordinates and orientations should be determinable with high reliability and precision. This will permit individual RyRs to be "isolated" computationally from the tomograms and then to be averaged. Averaged RyRs will reveal the presence of protein components that interact directly with them. In this manner a much more detailed picture of the interactions of the RyR with TT components will emerge.

Another way to increase the information attainable from cryotomography would be to label the specimens with electron-dense probes that are specific for triadic components. For example, we have added calmodulin that was labeled with a 1.4-nm diameter gold cluster (Wagenknecht et al., 1994) to isolated triads and found that the gold cluster could be identified in micrographs of frozen-hydrated specimen (unpublished data). Similarly, we envision that gold cluster-labeled antibodies specific for triad components could offer a general approach to identify the locations of the components with a precision that is not possible with conventional immunoelectron microscopy.

REFERENCES

Agrawal, R. K., and J. Frank. 1999. Structural studies of the translational apparatus. *Curr. Opin. Struct. Biol.* 9:215–221.

Anderson, K., and G. Meissner. 1995. T-tubule depolarization-induced SR Ca^{2+} release is controlled by dihydropyridine receptor- and Ca^{2+}-dependent mechanisms in cell homogenates from rabbit skeletal muscle. *J. Gen. Physiol.* 105:363–383.

Baumeister, W., R. Grimm, and J. Walz. 1999. Electron tomography of molecules and cells. *Trends Cell Biol.* 9:81–85.

Baumeister, W., and A. C. Steven. 2000. Macromolecular electron microscopy in the era of structural genomics. *Trends Biochem. Sci.* 25:624–631.

Block, B. A., T. Imagawa, K. P. Campbell, and C. Franzini-Armstrong. 1988. Structural evidence for direct interaction between the molecular components of the transverse tubule/sarcoplasmic reticulum junction in skeletal muscle. *J. Cell Biol.* 107:2587–2600.

Böhm, J., A. S. Frangakis, R. Hegerl, S. Nickell, D. Typke, and W. Baumeister. 2000. Toward detecting and identifying macromolecules in a cellular context: template matching applied to electron tomograms. *Proc. Natl. Acad. Sci. U. S. A.* 97:14245–14250.

Brandt, N. R., and A. H. Caswell. 1999. Localization of mitsugumin 29 to transverse tubules in rabbit skeletal muscle. *Arch. Biochem. Biophys.* 371:348–350.

Brunschwig, J. P., N. R. Brandt, A. H. Caswell, and D. S. Lukeman. 1982. Ultrastructural observations of the junctional foot protein and dihydropyridine receptor in skeletal muscle by use of tannic acid mordanting. *J. Cell Biol.* 93:533–542.

Caswell, A. H., Y. H. Lau, and J.-P. Brunschwig. 1976. Ouabain-binding vesicles from skeletal muscle. *Arch. Biochem. Biophys.* 176:417–430.

Chiu, W., A. Mcgough, M. B. Sherman, and M. F. Schmid. 1999. High-resolution electron cryomicroscopy of macromolecular assemblies. *Trends Cell Biol.* 9:154–159.

Corbett, A. M., J. Bian, J. B. Wade, and M. F. Schneider. 1992. Depolarization-induced calcium release from isolated triads measured with impermeant Fura-2. *J. Membr. Biol.* 128:165–179.

Costello, B., C. Chadwick, A. Saito, A. Chu, A. Maurer, and S. Fleischer. 1986. Characterization of the junctional face membrane from terminal cisternae of sarcoplasmic reticulum. *J. Cell Biol.* 103:741–753.

Crowther, R. A., D. J. DeRosier, and A. Klug. 1970. The reconstruction of a three-dimensional structure from projections and its application to electron microscopy. *Proc. Roy. Soc. Lond. A*. 317:319–340.

Dierksen, K., D. Typke, R. Hegerl, J. Walz, E. Sackmann, and W. Baumeister. 1995. Three-dimensional structure of lipid vesicles embedded in vitreous ice and investigated by automated electron tomography. *Biophys. J.* 68:1416–1422.

Dubochet, J., M. Adrian, J.-J. Chang, J.-C. Homo, J. Lepault, A. W. McDowall, and P. Schultz. 1988. Cryo-electron microscopy of vitrified specimens. *Quart. Rev. Biophys.* 21:129–228.

Dubochet, J., and N. Sartori Blanc. 2001. The cell in absence of aggregation artifacts. *Micron.* 32:91–99.

Dulhunty, A. F. 1989. Feet, bridges, and pillars in triad junctions of mammalian skeletal muscle: their possible relationship to calcium buffers in terminal cisternae and T-tubules and to excitation-contraction coupling. *J. Membr. Biol.* 109:73–83.

Ferguson, D. G., H. W. Schwartz, and C. Franzini-Armstrong. 1984. Subunit structure of junctional feet in triads of skeletal muscle: a freeze-drying, rotary-shadowing study. *J. Cell Biol.* 99:1735–1742.

Flucher, B. E., and C. Franzini-Armstrong. 1996. Formation of junctions involved in excitation-contraction coupling in skeletal and cardiac muscle. *Proc. Natl. Acad. Sci. U. S. A.* 93:8101–8106.

Franzini-Armstrong, C. 1980. Structure of the sarcoplasmic reticulum. *Fed. Proc.* 39:2403–2409.

Franzini-Armstrong, C. 1994. The sarcoplasmic reticulum and the transverse tubules. *In* Myology: Basic and Clinical. A.G. Engel and C. Franzini-Armstrong, editors. McGraw-Hill, Inc., New York. 176–199.

Franzini-Armstrong, C., and A. O. Jorgensen. 1994. Structure and development of E-C coupling units in skeletal muscle. *Annu. Rev. Physiol.* 56:509–534.

Franzini-Armstrong, C., L. J. Kenney, and E. Varriano-Marston. 1987. The structure of calsequestrin in triads of vertebrate skeletal muscle: a deep-etch study. *J. Cell Biol.* 105:49–56.

Grabner, M., R. T. Dirksen, N. Suda, and K. G. Beam. 1999. The II-III loop of the skeletal muscle dihydropyridine receptor is responsible for the bi-directional coupling with the ryanodine receptor. *J. Biol. Chem.* 274:21913–21919.

Grimm, R., H. Singh, R. Rachel, D. Typke, W. Zillig, and W. Baumeister. 1998. Electron tomography of ice-embedded prokaryotic cells. *Biophys. J.* 74:1031–1042.

Gulbis, J. M., M. Zhou, S. Mann, and R. MacKinnon. 2000. Structure of the cytoplasmic β subunit-T1 assembly of voltage-dependent K^+ channels. *Science.* 289:123–127.

Hsieh, C., M. Marko, J. Frank, and C. Mannella. 2002. Electron tomographic analysis of frozen-hydrated tissue sections. *J. Struct. Biol.* 138:63–73.

Ikemoto, N., B. Antoniu, and D. H. Kim. 1984. Rapid calcium release from the isolated sarcoplasmic reticulum is triggered via the attached transverse tubular system. *J. Biol. Chem.* 259:13151–13158.

Ikemoto, N., D. H. Kim, and B. Antoniu. 1988. Measurement of calcium release in isolated membrane systems: coupling between the transverse tubule and sarcoplasmic reticulum. *Method. Enzymol.* 157:469–480.

Inui, M., A. Saito, and S. Fleischer. 1987. Purification of the ryanodine receptor and identity with feet structures of junctional terminal cisternae of sarcoplasmic reticulum from fast skeletal muscle. *J. Biol. Chem.* 262:1740–1747.

Jorgensen, A. O., A. C. Shen, K. P. Campbell, and D. H. MacLennan. 1983. Ultrastructural localization of calsequestrin in rat skeletal muscle by immunoferritin labeling of ultrathin frozen sections. *J. Cell Biol.* 97:1573–1581.

Kawamoto, R. M., J.-P. Brunschwig, and A. H. Caswell. 1988. Localization by immunoelectron microscopy of spanning protein of triad junction in terminal cisternae/triad vesicles. *J. Muscle Res. Cell Motil.* 9:334–343.

Kim, D. H., S. T. Onhishi, and N. Ikemoto. 1983. Kinetic studies of calcium release from sarcoplasmic reticulum in vitro. *J. Biol. Chem.* 258:9662–9668.

Kim, K. C., A. H. Caswell, J.-P. Brunschwig, and N. R. Brandt. 1990. Identification of a new subpopulation of triad junctions isolated from skeletal muscle, morphological correlations with intact muscle. *J. Membr. Biol.* 113:221–235.

Kobertz, W. R., C. Williams, and C. Miller. 2000. Hanging gondola structure of the T1 domain in voltage-gated K^+ channel. *Biochemistry.* 39:10347–10352.

Koster, A. J., R. Grimm, D. Typke, R. Hegerl, A. Stoschek, J. Walz, and W. Baumeister. 1997. Perspectives of molecular and cellular electron tomography. *J. Struct. Biol.* 120:276–308.

Kramer, J. W., and A. M. Corbett. 1996. Comparison of Ca^{2+} loading and retention in isolated skeletal muscle triads and terminal cisternae. *Am. J. Physiol.* 270:C1602–C1610.

McEwen, B. F., and M. Marko. 2001. The emergence of electron tomography as an important tool for investigating cellular architecture. *J. Histochem. Cytochem.* 49:553–563.

Mackrill, J. J. 1999. Protein-protein interactions in intracellular Ca^{2+}-release channel function. *Biochem. J.* 337:345–361.

Mannella, C. A., C.-E. Hsieh, and M. Marko. 1999. Electron microscopic tomography of whole, frozen-hydrated rat-liver mitochondria at 400 kV. *Microsc. Microanal.* 5:416–417.

Marko, M., and A. Leith. 1996. Sterecon–three-dimensional reconstructions from stereoscopic contouring. *J. Struct. Biol.* 116:93–98.

Maurer, A., M. Tanaka, T. Ozawa, and S. Fleischer. 1985. Purification and crystallization of the calcium binding protein of sarcoplasmic reticulum from skeletal muscle. *Proc. Natl. Acad. Sci. U.S.A.* 82:4036–4040.

Mitchell, R. D., A. Saito, P. Palade, and S. Fleischer. 1983. Morphology of isolated triads. *J. Cell Biol.* 96:1017–1029.

Nakai, J., R. T. Dirksen, H. T. Nguyen, I. N. Pessah, K. G. Beam, and P. D. Allen. 1996. Enhanced dihydropyridine receptor channel activity in the presence of ryanodine receptor. *Nature.* 380:72–75.

Nakai, J., N. Sekiguchi, T. A. Rando, P. D. Allen, and K. G. Beam. 1998. Two regions of the ryanodine receptor involved in coupling with L-type Ca^{2+} channels. *J. Biol. Chem.* 273:13403–13406.

Nicastro, D., A. S. Frangakis, D. Typke, and W. Baumeister. 2000. Cryo-electron tomography of *Neurospora* mitochondria. *J. Struct. Biol.* 129:48–56.

Nogales, E., and N. Grigorieff. 2001. Molecular machines: putting the pieces together. *J. Cell Biol.* 152:F1–F10.

Penczek, P., M. Marko, K. Buttle, and J. Frank. 1995. Double-tilt tomography. *Ultramicroscopy.* 60:393–410.

Radermacher, M., V. Rao, R. Grassucci, J. Frank, A. P. Timerman, S. Fleischer, and T. Wagenknecht. 1994. Cryo-electron microscopy and three-dimensional reconstruction of the calcium release channel ryanodine receptor from skeletal muscle. *J. Cell Biol.* 127:411–423.

Rath, B. K., M. Marko, M. Radermacher, and J. Frank. 1997. Low-dose automated electron tomography: a recent implementation. *J. Struct. Biol.* 120:210–218.

Ruiz, T., I. Erk, and J. Lepault. 1994. Electron cryo-microscopy of vitrified biological specimens: towards high spatial and temporal resolution. *Biol. Cell.* 80:203–210.

Saito, A., M. Inui, M. Radermacher, J. Frank, and S. Fleischer. 1988. Ultrastructure of the calcium release channel of sarcoplasmic reticulum. *J. Cell Biol.* 107:211–219.

Saito, A., S. Seiler, A. Chu, and S. Fleischer. 1984. Preparation and morphology of sarcoplasmic reticulum terminal cisternae from rabbit skeletal muscle. *J. Cell Biol.* 99:875–885.

Sato, C., Y. Ueno, K. Asai, K. Takahashi, M. Sato, A. Engel, and Y. Fujiyoshi. 2001. The voltage-sensitive sodium channel is a bell-shaped molecule with several cavities. *Nature.* 409:1047–1051.

Serysheva, I. I., E. V. Orlova, W. Chiu, M. B. Sherman, S. L. Hamilton, and M. van Heel. 1995. Electron cryomicroscopy and angular reconstitution used to visualize the skeletal muscle calcium release channel. *Struct. Biol.* 2:18–24.

Sokolova, O., L. Kolmakova-Partensky, and N. Grigorieff. 2001. Three-dimensional structure of a voltage-gated potassium channel at 2.5 nm resolution. *Structure.* 9:215–220.

Stewart, P. S., and D. H. MacLennan. 1974. Surface particles of sarcoplasmic reticulum membranes: structural features of the adenosine triphosphatase. *J. Biol. Chem.* 249:985–993.

Takekura, H., L. Bennett, T. Tanabe, K. G. Beam, and C. Franzini-Armstrong. 1994. Restoration of junctional tetrads in dysgenic myotubes by dihydropyridine receptor cDNA. *Biophys. J.* 67:793–803.

Takeshima, H., S. Komazaki, M. Nishi, M. Iino, and K. Kangawa. 2000. Junctophilins: a novel family of junctional membrane complex proteins. *Mol. Cell.* 6:11–22.

Takeshima, H., M. Shimuta, S. Komazaki, K. Ohmi, M. Nishi, A. Miyata, and K. Kangawa. 1998. Mitsugumin29, a novel synaptophysin family member from the triad junction in skeletal muscle. *Biochem. J.* 331:317–322.

Wagenknecht, T., J. Berkowitz, R. Grassucci, A. P. Timerman, and S. Fleischer. 1994. Localization of calmodulin binding sites on the ryanodine receptor from skeletal muscle by electron microscopy. *Biophys. J.* 67:2286–2295.

Wagenknecht, T., R. Grassucci, and J. Frank. 1988. Electron microscopy and computer image averaging of ice-embedded large ribosomal subunits from *Escherichia coli*. *J. Mol. Biol.* 199:137–147.

Wagenknecht, T., M. Radermacher, R. Grassucci, J. Berkowitz, H.-B. Xin, and S. Fleischer. 1997. Locations of calmodulin and FK506-binding protein on the three-dimensional architecture of the skeletal muscle ryanodine receptor. *J. Biol. Chem.* 272:32463–32471.

Zhang, L., J. Kelley, G. Schmeisser, Y. M. Kobayashi, and L. R. Jones. 1997. Complex formation between junctin, triadin, calsequestrin, and the ryanodine receptor: proteins of the cardiac junctional sarcoplasmic reticulum membrane. *J. Biol. Chem.* 272:23389–23397.